Effectiveness of On-site Dielectric Test of GIS Equipment

Zhicheng Wu, Qiaogen Zhang, Jingtan Ma, Xiaoang Li and **Tao Wen**
State Key Laboratory of Electric Insulation and Power Equipment
Xi'an Jiaotong University
Xi'an, 710049, P.R.China

ABSTRACT

Even for gas-insulated metal-enclosed switchgear (GIS) equipment that has passed an on-site dielectric test, some dielectric failure can occasionally occur without warning. It is necessary to evaluate the effectiveness of on-site dielectric tests of GIS equipment. In this study, two standard test procedures, power-frequency partial discharge (PD) and lighting impulse (LI) withstand test, were carried out in a real model test platform of 550 kV GIS to evaluate the effectiveness of on-site dielectric tests. Through experiments, the minimum detectable defect sizes were determined for different curvature radius values. The results show the limitation of the power-frequency PD test and the need to use of the LI withstand test as supplementary assessment on site. Two calculable constraints of defect detectability were proposed to extend the results to GIS equipment at other voltage levels. The results clarify the cause of dielectric failure without any warning and provide technological guidance for manufacturing and installation.

Index Terms—**Gas insulation, GIS equipment failure, partial discharges, impulse testing.**

1 INTRODUCTION

DUE to the rapid increase of electricity demand and the voltage level of power equipment, there are increased requirements for reliability of gas-insulated metal-enclosed switchgear (GIS) equipment widely used in power systems. In the manufacture, installation and commission process of GIS equipment, insulation defects may appear, and can include conductor protrusions and roughness, free conductive particles and other electric field concentration defects [1-4]. These defects may cause abnormal discharge during normal operation or overvoltage, threatening the safe and stable operation of the system [5].

In order to minimize effects on dielectric integrity, full-coverage tests, including type tests, routine tests, on-site tests and online-monitoring, are typically performed throughout the total life cycle of GIS equipment [6, 7]. The equipment is put into service after the on-site dielectric tests. These tests assess the dielectric integrity, and are necessary to determine the reliability of GIS equipment [8].

Although every newly installed GIS is subjected to an on-site dielectric test, some dielectric failure may occasionally occur. For instance, a sudden shut-down accident of the GIS tubular busbar in the Three Gorges hydropower station that occurred during normal operation was the result of a discharge fault of the conductor. There was no abnormal change detected by the online monitoring performed post-accident [9]. Obviously, it is necessary to evaluate the effectiveness of on-site dielectric tests of GIS equipment.

In this study, two standard test procedures were carried out using a real model test platform of 550 kV GIS to evaluate the effectiveness of on-site dielectric tests according to IEC 62271-203. The minimum detectable defect sizes were determined experimentally for different curvature radius values. The results show the limitations of the power-frequency partial discharge (PD) test and the requirement of the supplementary of lightning impulse (LI) withstand test for online testing. Based on these results, two calculable constraints of defects detectability were proposed to extend the results to GIS equipment operating at other voltage levels.

2 EXPRIMENTAL CONDITIONS

2.1 EXPRIMENTAL METHOD

According to IEC 62271-203, two on-site dielectric test procedures are recommended for 245 kV and above [10]. The first test procedure is a power-frequency voltage test performed for 1 min duration, followed by the PD test. As the alternative to the first test procedure, the second procedure is a short-duration power-frequency voltage test followed by LI tests with three impulse at each polarity. The principle of these two test procedures to detect dielectric integrity is different: The partial discharge test judges the dielectric integrity by

Manuscript received on 1 February 2018, in final form 3 May 2018, accepted 3 May 2018. Corresponding author: Q. Zhang.

detecting weak discharges under AC voltage; the lightning impulse withstand test uses the steep-front impulse voltage. For a 550 kV GIS, the IEC recommend on-site dielectric test voltages are shown in Table 1.

TABLE 1. On-site Dielectric Test Voltages for 550 kV GIS.

Tests	Test Voltage (kV)
Power-frequency short-duration withstand test	560 (r.m.s. value)
Power-frequency PD test	385 (r.m.s. value)
Lightning impulse withstand test	1240

The power-frequency short-duration withstand test is needed, so its effectiveness of this test is not analyzed here.

During the power-frequency PD test, U_{ds} was applied for 1 min, and then the test voltage was reduced to U_{pd}. PD signals were recorded for 5 min. According to IEC 62271-203, PD measurement method should be compliant with IEC 60270, and the threshold of the apparent charge is 10 pC. If the maximum of apparent charge quantity within 5 min exceeds this threshold, the defect is detected.

During the LI withstand test, U_{ps} was applied three times for each polarity. If any breakdown occurs, the defect is detected.

To reduce the effect of the earlier experiments on the experimental results, sequential experiments were separated by 10 min.

To evaluate the effectiveness of a specific test procedure, the defect size was adjusted continuously until the defect could be detected. This process can be accelerated by using an interval halving of dichotomy method. The minimum detectable defect size is defined as the critical length l_{cr}, such that the defect can be detected if its size is greater than this critical length.

2.2 EXPERIMENTAL CIRCUIT

A real model test platform of 550 kV GIS was used in these experiments and is shown in Figure 1. In order to apply different test procedure to the same experimental chamber, a disconnecting switch/earthing switch (DS/ES) was used to switch the test voltage source.

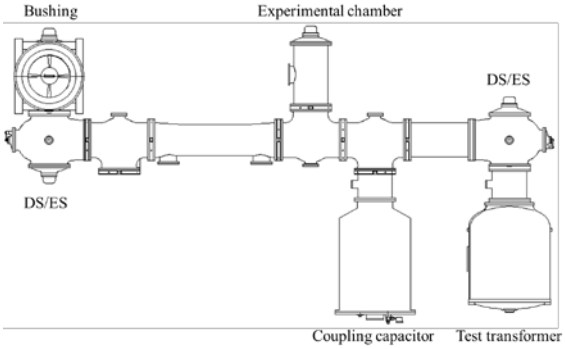

Figure 1. Diagram of real model test platform of GIS for 550kV rated voltage.

On the one hand, the experimental chamber was connected to a 550 kV/250 kVA corona-free test transformer via a basin-type spacer during the power frequency test. Using a non-corona design, the test transformer can maintain its own PD charge at less than 1 pC under 550 kV. The voltage is measured by a capacitive voltage divider, and its combined standard uncertainty does not exceed 5% [11-13]. The Omicron MPD600 system is IEC 60270-compliant and was used as the PD measurement system [14]. Its fully digital data processing technique allowed high measurement accuracy was ensured. The PD signal was detected by a 550 kV/500 pF coupling capacitor, measuring impendence CPL542 and measurement unit MPD600, etc. The charge calibrator CAL542 was used to calibrate the apparent charge in parallel with the experimental chamber. The measurement system provided a reference with a noise level equivalent to less than 1 pC.

On the other hand, the experimental chamber was connected to 1600 kV impulse voltage generator via a 550 kV bushing during the LI withstand test. The standard LI voltage waveform (1.2/50 μs) was adopted in this test, and the voltage was measured by a capacitor divider with a voltage ratio of 20,000: 1 and a combined standard uncertainty of 5%.

2.3 DEFECT SIMULATION

Electric field concentration is regarded as a common defect in GIS equipment. Protrusions can be fixed on the busbar to simulate electric field concentration, and the electrode system used here is shown in Figure 2. Because the protrusions are directly on the busbar, the polarity of PDs is the same as the polarity of the applied voltage.

For a 550 kV GIS, the radius of enclosure R_1 is 280 mm, and the radius of the busbar R_2 is 70 mm. The surface roughness of the busbar is controlled below 30 μm to avoid rough electrode surface effect on discharge characteristics. [15]. Due to varying degrees of electric field concentration, steel needle electrodes with a curvature radius r of 250, 300, 375, 450 and 500 μm were used in this study. The protrusions length l can be adjusted from 0 to 20 mm.

Before the experiment, the experimental chamber was evacuated to vacuum, and then it was filled with 0.5 MPa SF_6 gas to maintain consistent operating condition.

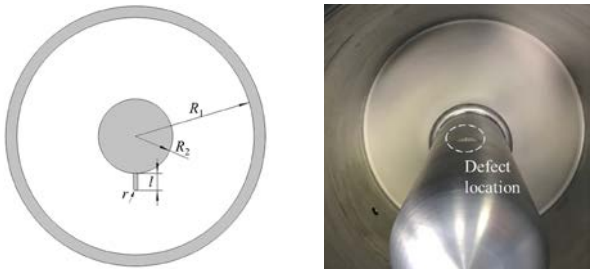

(a) Diagram (b) Photo

Figure 2. Electrode system.

3 RESULTS

3.1 CRITICAL LENGTH OF POWER-FREQUENCY PD TEST

After a series of power-frequency PD tests, the critical length $l_{cr\text{-}pd}$ was obtained, as shown in Figure3. The critical length $l_{cr\text{-}pd}$ decreased first and then increased with the curvature radius, showed a non-monotonous phenomenon. The results indicates that there is a demarcation point approximately at a curvature radius of 375 μm. Not all dielectric defect can be detected on on-site dielectric test. The area above the curve indicates the detectable defects.

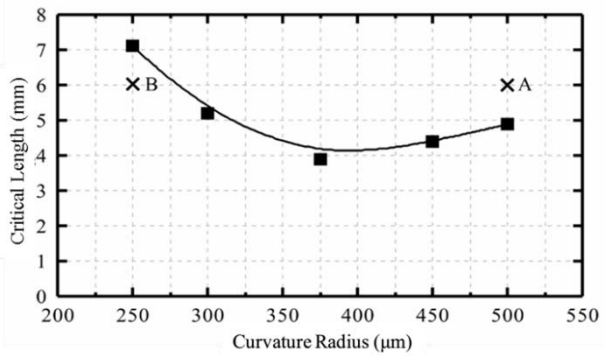

Figure 3. Critical length of the power-frequency PD test as a function of curvature radius, note the non-monotonous trend.

In order to explain this non-monotonous phenomenon, phase-resolved partial discharge (PRPD) patterns were measured under varying applied voltage as shown in Figure 4.

Figure 4a shows the relationship between the PRPD pattern and applied voltage for a curvature radius greater than 375 μm. Faint PDs first occur in the negative half period at 310 kV. The PD charge increased slowly with PDs still appearing in the negative half period. The positive half period PDs appeared suddenly when the applied voltage reached 350 kV. The PD charge was usually greater than 10 pC once PDs occur in the positive half period. Thus, for a large curvature radius, the detectability of defects depends on whether the test voltage U_{pd} is greater or less than the positive streamer onset voltage.

Figure 4b shows the other mode of PRPD pattern for a curvature radius smaller than 375 μm. The defect cannot be detected under this condition. Because of the high stress caused by a sharper protrusion, the PD inception voltage was lower under this condition compared to that seen above. Faint but frequent PDs occur in both polarities over a wide range. The PD charge was less than 10 pC when the applied voltage reached U_{pd}. Hence, for a small curvature radius, the detectability of defects depends on whether the PD charge is greater or less than 10 pC under U_{pd}.

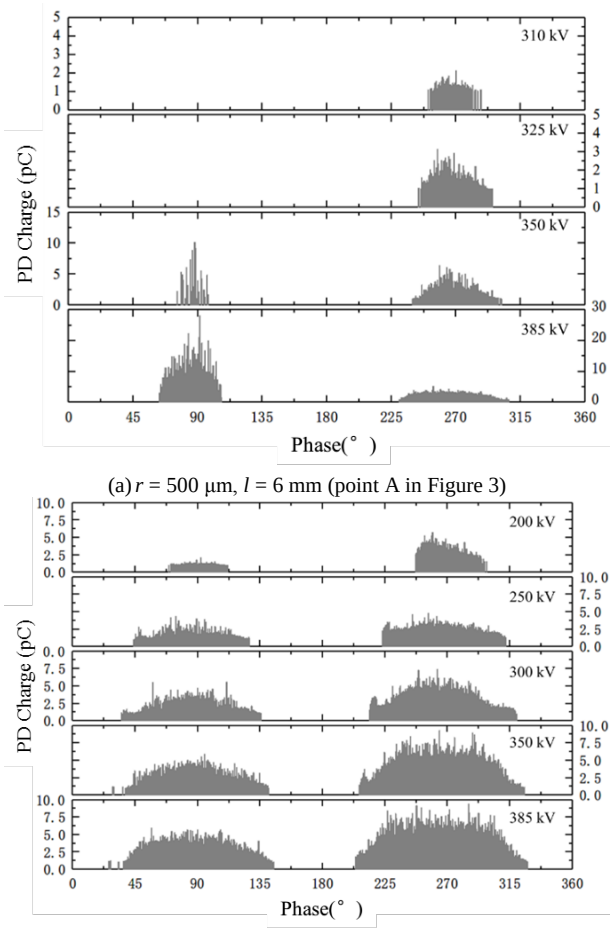

Figure 4. PRPD pattern as a function of applied voltage of different defect size, noted that distinct modes appear in (a) and (b).

The reason for the non-monotonous phenomenon is the distribution of the electric field. As illustrated by the schematic diagram in Figure 5. For a protrusion with a small curvature radius, the electric field strength in front of the protrusion is sufficiently high, but it decays rapidly with distance. The ionization zone is too small to provide enough space for streamer propagation. In contrast, the decay of the electric field is much slower for a larger curvature radius. The positive streamer can continue to propagate if the electric field strength greater than critical electric field strength E_{cr}. Under this circumstance, the PD charge is generally greater than 10 pC.

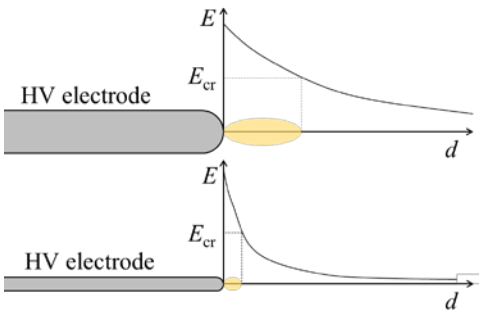

Figure 5. Schematic diagram of interpretation about PD charge and curvature radius.

3.2 CRITICAL LENGTH OF LI WITHSTAND TEST

After a series of LI withstand tests, the critical length $l_{cr\text{-}LI}$ was obtained as shown in Figure 6. Different from the results of the power-frequency PD test, the results showed that $l_{cr\text{-}LI}$ was monotonic over changing curvature radius, and the smaller curvature radius, the shorter the critical length. For an extremely short protrusion size (l <1 mm), the decline trends becomes saturated because of the shield effect of the busbar.

There was an obvious difference between positive polarity and negative polarity [16]. In this study, the protrusion was located on the busbar, so it is not reasonable to interpret the data as showing that a positive LI is a better detection method. In contrast, if there is a protrusion at the enclosure, the critical length for a negative LI will be smaller than for a positive LI. Therefore, it is necessary to apply impulses of both polarities during the on-site dielectric test.

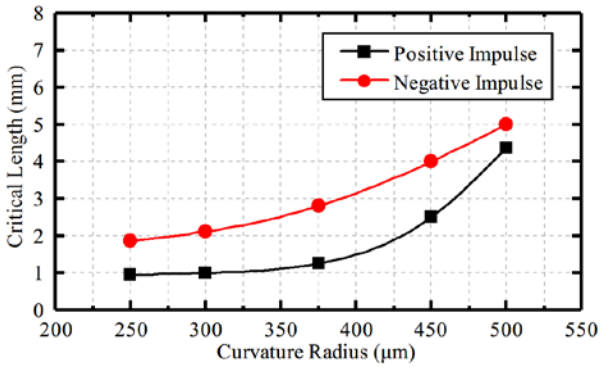

Figure 6. Critical length of LI withstand test as a function of curvature radius, note the consistent trend.

4 DISCUSSION

First of all, a comparison is made of these two test procedures. Then the calculation of the power-frequency PD blind zone of detectability is discussed in order to extend the results to GIS equipment of other voltage levels.

4.1 COMPARISON WITH TWO TEST PROCEDURES

For the 550 kV GIS equipment, the critical lengths determined by these two procedures are as shown in Figure 7. The minimum detectable defect sizes of the power-frequency PD test and the LI withstand test were 4 mm and 1 mm, respectively. Obviously, the critical length of the LI withstand test was less than the critical length of the power-frequency PD test. Thus, the LI withstand test is more effective than the power-frequency PD test at least for the electric field concentration defect tested here.

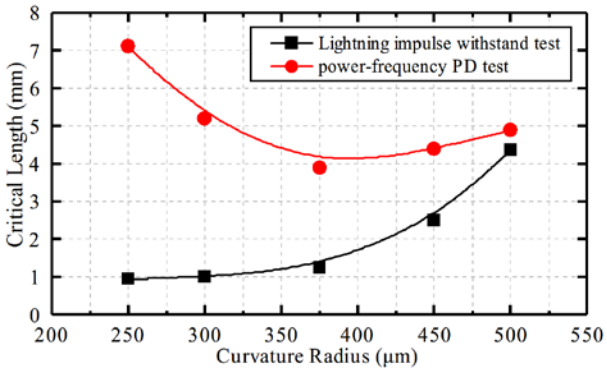

Figure 7. Critical length of both tests as a function of curvature radius.

Is it possible to use LI withstand test instead of power-frequency PD test? Obviously, the answer is NO. Because of the dual constraint of the PD onset condition and the PD charge condition, the power-frequency PD test shows a notable limitation. On the one hand, some defects, including floating electrodes and free conductive particles, can be detected effectively by this test because power-frequency voltage is a kind of steady-state voltage. On the other hand, the lightning impulse withstand test is invalid for these insulation defects. The PD threshold is 10 pC as set by the current standard, and is limited by noise on site. Advances in PD noise reduction technology and PD identification technology can effectively reduce this threshold [17, 18].

Based on the development of new types of compact impulse voltage generators with low inductance, the use of on-site testing of standard LI for power equipment with large capacitance will be possible [19].

In summary, not only the power-frequency PD test, but also the LI withstand test should be carried out as supplementary on site.

4.2 CALCULATION OF POWER-FREQUENCY PD BLIND ZONE OF DETECTABILITY

In this section, the power-frequency PD blind zone of detectability is calculated, and the calculation and the experimental results show acceptable consistency. According to the above analysis, the blind zone can be calculated using the onset voltage calculation and the PD charge calculation to extend the results to GIS equipment of another voltage level.

Based on the theories established by M. Abdel-Salam, the positive streamer onset voltage can be calculated by Equation (1), considering the effect of photoionization [20]. Once the size of successor avalanches N_2 just exceeds the size of primary avalanche N_1, the discharge process becomes self-sustained. The size of avalanches is calculated as outlined in Appendix. The applied voltage corresponding this physics process is the positive streamer onset voltage.

$$N_2 \geq N_1 \tag{1}$$

The length of the protrusion can be adjusted continuously until the positive streamer onset voltage is exactly equal to U_p. This length can be regarded as the critical length, because the onset positive streamer can be detected immediately for a large

curvature radius.

To estimate the calculating PD charge, a starting point is to expand the scope of the application of discharge self-sustained criterion. The size of the avalanche is considered a source of PD charge. Based on the above hypothesis, an electric field operator is defined to describe the avalanche size as written in Equation (2).

$$\Gamma(E)=\exp(\int_{x_c}(\alpha-\eta)\,\mathrm{d}x) \tag{2}$$

Extracting the maximum of PD charge q_{max} from the series of experiments with different protrusion size and different applied voltage, the relationship between Γ and q_{max} was determined and is shown as Figure 8. The value of q_{max} increased linearly with Γ for a specific curvature radius. Hence, the PD charge can be estimated by Equation (3). The constant K can be obtained by fitting the scatter data in Figure 8.

$$q_{max}=\mathrm{K}\Gamma \tag{3}$$

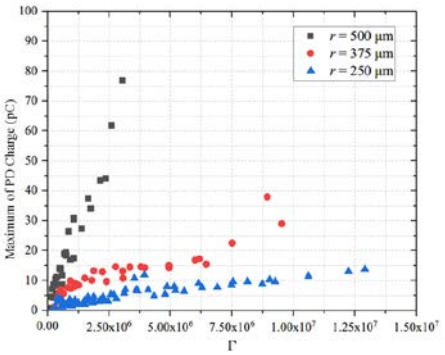

Figure 8. Maximum of PD charge as a function of electric field operator Γ.

According to the calculation of positive streamer onset voltage and PD charge, the calculated PD onset constraint and PD charge constraint is shown by the dashed lines in Figure 9. The experimental results are represented by the dots in the Figure 9. We considered that the calculation is in acceptable agreement with the experimental results. A defect can be detected if its size parameter is located within the green zone. Along the curvature radius axis, the PD charge constraint line and the PD onset constraint line showed a reverse trend. These two constraint lines intersect at one point, i.e. the demarcation point as mentioned above.

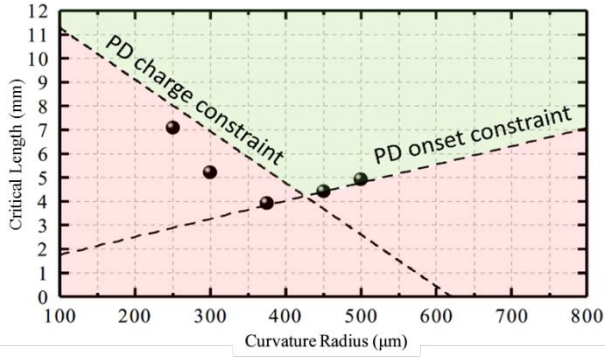

Figure 9. The calculation and the experimental results of the power-frequency PD blind zone of detectability.

5 CONCLUSIONS

To clarify the cause of dielectric failure of GIS equipment without any warning, this study evaluated the effectiveness of on-site dielectric test. Two standard test procedures, in strict conformity with IEC 62271-203, were carried out to determine the minimum detectable defect size. The results are summarized as follows:

1) No matter what test procedure is chosen, not all dielectric defect can be detected on the on-site dielectric test.

2) The critical length of the power-frequency PD test shows a non-monotonous trend as it decreases first and then increases with the curvature radius. The critical length of the LI withstand test was consistent with varying curvature radius. The smaller the curvature radius is, the shorter the critical length. Thus, the LI withstand test is more effective than the power-frequency PD test during on-site dielectric test at least for the electric field concentration defect in this study.

3) In the power-frequency PD test, the detectability of defects depends on whether the test voltage U_{pd} is greater or lower than the positive streamer onset voltage for a large curvature radius. The detectability of defects depends on whether the PD charge is greater or lower than 10 pC under U_{pd} for a small curvature radius. The blind zone of detectability can be determined by onset voltage calculation and PD charge calculation to extend the results to GIS equipment of another voltage level.

APPENDIX

The set of equations describing the size of the primary avalanche N_1 and the successor avalanches N_2 is as follows in Equation (4). The ranges of integration of Equation (4) are described in Figure 10.

$$\begin{aligned} N_1&=e^{\int_{z_s}^{z_i}\bar{\alpha}\mathrm{d}z}\\ N_2&=\int_{z_i}^{r_e} gf_1f_2N_1\mu e^{-\mu\rho}e^{\int_{\rho}^{r_e}\bar{\alpha}\mathrm{d}z}\mathrm{d}\rho \end{aligned} \tag{4}$$

The ionization and attachment coefficients $\bar{\alpha}$ of SF_6 is as follows:

$$\frac{\bar{\alpha}}{p}=0.0262(\frac{E}{p}-87.6) \tag{5}$$

The influence of electric field strength due to the space charge of the primary avalanche should be considered. The space charge is regarded as a point charge in front of the HV electrode. The electric field strength can be calculated by Equation (6).

$$\begin{aligned} E_s&=\frac{eN_1}{4\pi\varepsilon_0(z-r_e)^2},z>2r_e\\ E_s&=0,z\le 2r_e \end{aligned} \tag{6}$$

The radius of the primary avalanche r_e is as follows:

$$r_e=\sqrt{6D_et} \tag{7}$$

The electron transit time t is expressed as

$$t = \int_{z_s}^{z_i} \frac{1}{V_e} dz \tag{8}$$

The transport coefficients of SF_6 is as follows:

$$V_e = 1.027 \times 10^{19} \left(\frac{E}{N}\right)^{0.7424} \tag{9}$$

$$D_e = \frac{V_e}{E} \cdot 8.6488 \times 10^9 \left(\frac{E}{N}\right)^{\frac{1}{2}} \tag{10}$$

The meanings and values of other symbols are shown in Table 2.

TABLE 2. Definitions of symbols used and values.

Symbol	Definition	Value
g	geometry factor	$g = 0.5$
f_1	number of photo electrons released by absorption of one photon	$f_1 \cdot f_2 = 6 \times 10^{-6}$
f_2	number of excited states production per ionizing collision	
μ	photon absorption coefficient	$\mu = 0.789p$

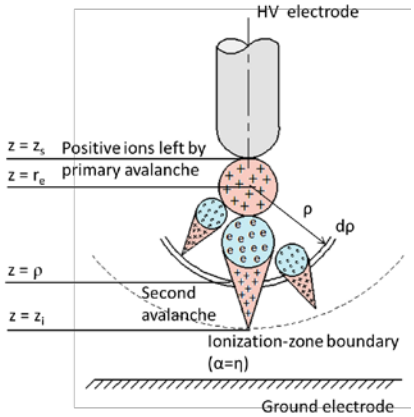

Figure 10. Schematic of the positive streamer onset model.

REFERENCES

[1] M. Runde, "Failure Frequencies for High-Voltage Circuit Breakers, Disconnectors, Earthing Switches, Instrument Transformers, and Gas-Insulated Switchgear," IEEE Trans. Dielectr. Electr. Insul., vol. 28, pp. 529–530, Jan. 2013.

[2] S. Dekic, P. Osmokrovic, M. Vujisic and K. Stankovic, "Conditions for the applicability of the geometrical similarity law to impulse breakdown in gases," IEEE Trans. Dielectr. Electr. Insul., vol. 17, pp. 1185–1195, Aug. 2010.

[3] Z. Milanovic, K. Stankovic, M. Vujisic, R. Radosavljevic and P Osmokrovic, "Calculation of impulse characteristics for gas-insulated systems with homogenous electric field," IEEE Trans. Dielectr. Electr. Insul., vol. 19, pp. 648–659, Apr. 2012.

[4] P. Osmokrovic， M. Stojkanovic， K. Stankovic， M. Vujisic and D. Kovacevic, "Synergistic effect of SF_6 and N_2 gas mixtures on the dynamics of electrical breakdown," IEEE Trans. Dielectr. Electr. Insul., vol. 19, pp. 677–688, Apr. 2012.

[5] CIGRE JWG 33/23.12, "Insulation Co-ordination of GIS: Return of Experience, On Site Tests and Diagnostic Techniques," Electra, vol. 176, pp. 67–97, Feb. 1999.

[6] T. Wen, Q. Zhang, L. Zhang, J. Ma, C. Guo, M. Chen, Y. Li, N. Shimomura and W. Chen, "Discussion on lightning impulse test waveform according to breakdown characteristics of SF_6 gas gaps," IEEE Trans. Dielectr. Electr. Insul., vol. 24, pp. 2306–2313, Sep. 1999.

[7] U. Schichler, W. Koltunowicz, F. Endo, K. Feser, A. Giboulet, A. Girodet, H. Hama, B. Hampton, H.-G Kranz, J. Lopez-Roldan, L. Lundgaard, S. Meijer, C. Neumann, S. Okabe, J. Pearson, R. Pietsch, U. Riechert and S. Tenbohlen, "Risk assessment on defects in GIS based on PD diagnostics," IEEE Trans. Dielectr. Electr. Insul., vol. 20, pp. 2165–2172, Dec. 2013.

[8] U. Schichler, W. Koltunowicz, D. Gautschi, A. Girodet, H. Hama, K. Juhre, J. Lopez-Roldan, S. Okabe, S. Neuhold, C. Neumann, J. Pearson, R. Pietsch, U. Riechert and S. Tenbohlen, "UHF partial discharge detection system for GIS: Application guide for sensitivity verification," IEEE Trans. Dielectr. Electr. Insul., vol. 23, pp. 1313-1321, Dec. 2016.

[9] L. Xu and S. Guan, "Analysis and Treatment of a Discharge Fault of GIL Tubular Busbar," Hydropower and New Energy, vol. 131, pp. 51–56, Feb. 2015.

[10] High-voltage Switchgear and Controlgear – Part 203: Gas-insulated Metal-enclosed Switchgear for Rated Voltages above 52 kV, IEC Standard 62271-203: 2011, 2011-09-07.

[11] P. Osmokrovic, D. Petkovic and O. Markovic, "Measuring probe for fast transients monitoring in gas insulated substation," IEEE Trans. Instrum. Meas., vol. 46, pp. 36–44, Feb. 1997.

[12] A. Kovacevic, D. Despotovic, Z. Rajovic, K. Stankovic, V. Kovacevic and U. Kovacevic, "Uncertainty evaluation of the conducted emission measurements," Nucl. Technol. Radiat., vol. 28, pp. 182–190, Jun. 2013.

[13] A. Kovacevic, A. Kovacevic, K. Stankovic and U Kovacevic, "The combined method for uncertainty evaluation in electromagnetic radiation measurement," Nucl. Technol. Radiat., vol. 29, pp. 279–284, Dec. 2014.

[14] High-voltage Test Techniques – Partial Discharge Measurements, IEC Standard 60270: 2015, 2015-11-27.

[15] P. Osmokrovic, M. Vujisic, K. Stankovic, A. Vasic and B. Loncar, "Mechanism of electrical breakdown of gases for pressures from 10-9 to 1 bar and inter-electrode gaps from 0.1 to 0.5 mm," Plasma Source Sci. T., vol. 16, pp. 643–655, Aug. 2007.

[16] J. Ma, Q. Zhang, H. You, Z. Wu, T. Wen, C. Guo, G. Wang and C. Gao, "Study on insulation characteristics of GIS under combined voltage of DC and lightning impulse," IEEE Trans. Dielectr. Electr. Insul., vol. 24, pp. 893–900, Dec. 2017.

[17] M. Zhu, Q. Liu, J. Xue, J. Deng, G. Zhang, X. Shao, W. He, A. Gu and X. Liu, "Self-adaptive separation of multiple partial discharge sources based on optimized feature extraction of cumulative energy function," IEEE Trans. Dielectr. Electr. Insul., vol. 24, pp. 246–258, Mar. 2017.

[18] J. M. Fresno, J. A. Ardila-Rey, J. M. Martínez-Tarifa and G. Robles, "Partial discharges and noise separation using spectral power ratios and genetic algorithms," IEEE Trans. Dielectr. Electr. Insul., vol. 24, pp. 31–38, Feb. 2017.

[19] T. Wen, Q. Zhang, Y. Qin, J. Zhao, J. Ma, Z. Wu, N. Shimomura, F. Tao, Y. Jia, Y. Yin, W. Shi and W. Chen, "On-site Standard Lightning Impulse Test for 1,100 kV Gas-insulated Switchgear with Large Capacitance," IEEE Elect. Insul. Mag., vol. 32, pp. 36 – 43, Nov. 2016.

[20] M. Abdel-Salam, A. A.Turky and A. A.Hashem, "The Onset Voltage of Coronas on Bare and Coated Conductors," J. Phys. D Appl. Phys., vol. 31, pp. 2550–2556, Jun. 1999

Zhicheng Wu was born in Yunnan, China in 1993. He received a B.S. degree in computer science and technology from Xi'an Jiaotong University, Shaanxi, China in 2015. He is currently working toward a Ph.D. degree in the High Voltage Division, School of Electrical Engineering, and the State Key Laboratory of Electrical Insulation and Power Equipment. His research interest is technology for defect detection of GIS/GIL.

Qiaogen Zhang received B.S., M.S., and Ph.D. degrees in electrical engineering from Xi'an Jiaotong University, Xi'an, China, in 1988, 1991, and 1996, respectively. He is currently a Professor with the High Voltage Division, School of Electrical Engineering, and the State Key Laboratory of Electrical Insulation and Power Equipment, Xi'an Jiaotong University. His major research interests include insulation structure design, power transmission and transformation technology and insulation state evaluation.

Jingtan Ma was born in Henan, China in 1993. He received the B.S. degree from Xi'an Jiaotong University, Shaanxi, China in 2014. He is currently working toward the Ph.D. degree at the High Voltage Division, School of Electrical Engineering, and the State Key Laboratory of Electrical Insulation and Power Equipment.

Xiaoang Li was born in Shaanxi Province, China, in May 1989. He received a B.S. degree and a Ph.D. degree in Electrical Engineering from Xi'an Jiaotong University, Xi'an, China, in 2011 and 2016 respectively. He is now a research assistant in the State Key Laboratory of Electrical Insulation and Power Equipment, Xi'an Jiaotong University, Xi'an, China. His mainly research interest is pulsed power technology and its applications.

Tao Wen was born in Shaanxi Province, China, in 1990. He received the BS degree and Ph.D. degree in electrical engineering from Xi'an Jiaotong University, Xi'an, China, in 2012 and 2017 respectively. He is currently a Post-doctor in the High Voltage Division, School of Electrical Engineering, and the State Key Laboratory of Electrical Insulation and Power Equipment, Xi'an Jiaotong University. He has also been working toward a doctoral double degree program at Tokushima University, Tokushima, Japan.